Dihedral Corner Reflector Backscatter Using Higher Order Reflections and Diffractions

TIMOTHY GRIESSER, STUDENT MEMBER, IEEE, AND CONSTANTINE A. BALANIS, FELLOW, IEEE

Abstract—**The uniform theory of diffraction (UTD) plus an imposed edge diffraction extension is used to predict the backscatter cross sections of dihedral corner reflectors which have right, obtuse, and acute included angles. UTD allows individual backscattering mechanisms of the dihedral corner reflectors to be identified and provides good agreement with experimental cross section measurements in the azimuthal plane. Multiply reflected and diffracted fields of up to third order are included in the analysis for both horizontal and vertical polarizations. The coefficients of the uniform theory of diffraction revert to Keller's original geometrical theory of diffraction (GTD) in far-field cross section analyses, but finite cross sections can be obtained everywhere by considering mutual cancellation of diffractions from parallel edges. Analytic calculations are performed using UTD coefficients; hence accuracy required in angular measurements is more critical as the distance increases. In particular, the common "far-field" approximation that all rays to the observation point are parallel is too gross of an approximation for the angular parameters in the UTD coefficients in the far field.**

I. Introduction

IN THE INTEREST of promoting the advancement of radar technology, engineers in past years have pursued methods to determine the backscatter characteristics of radar targets. Evaluating the radar echo strength of a particular target, as a function of the orientation of the target relative to the radar, has become a topic of major concern because the relative strength of the echo returned from a target can be related to the maximum distance at which that target can be detected or observed by a given radar system.

When considering the scattering properties of a conducting object, the two dominant mechanisms are reflections from surfaces and diffraction from edges. Understanding these mechanisms is important for the development of methods to reduce radar backscatter from ships, planes, missiles and spacecraft. The design of these "low-observable" vehicles, which are fabricated so as to reduce the possibility of radar detection, is often a complex task. However, in the future, the construction of nearly every new major military vehicle is expected to incorporate some form of radar cross section shaping.

One of the most popular methods for determining approximate scattered fields is the geometrical theory of diffraction (GTD) [1]–[6]. Originated by Keller [1], and refined as the uniform theory of diffraction (UTD) by Kouyoumjian and Pathak [2], GTD supplements geometrical optics by adding contributions due to edge diffraction at perfectly conducting edges. The theory has been used extensively, with much success, in many electromagnetic scattering problems [7]–[14]. UTD is especially useful because it provides good agreement with experimental results, it provides insight into specific scattering mechanisms, it involves common functions available on most computer systems, and solutions are relatively simple to construct in comparison to exact methods.

In this paper, UTD with an imposed edge diffraction extension is utilized to determine the backscatter cross sections of dihedral corner reflectors in the azimuthal plane. Through the dihedral corner reflector analysis, the versatility and accuracy of the theory can be evaluated. The dihedral corner reflector was chosen because it exhibits many of the scattering mechanisms of more complex bodies; namely strong specular reflections from singly, doubly, and triply reflected fields, along with significant first-, second-, and third-order diffracted fields. The dihedral corner reflector is analyzed here when the interior angle is right, acute, and obtuse.

Several papers have dealt with the study of a dihedral corner reflector using geometrical and physical theories. Yu and Huang [10] have compared vertical polarization computed patterns with measurements in the forward 180° region of the dihedral corner reflector using UTD. Knott [15] studied the backscattered fields of the obtuse dihedral corner reflector using a combination of geometrical and physical optics over the first 70° on each side of the forward direction, without incorporating diffraction terms. Michaeli [16] utilized physical diffraction in a study of the 90° dihedral corner reflector near grazing incidence to either plate. Griesser and Balanis [17] included physical optics and physical diffraction for right, obtuse, and acute dihedral corner reflectors over the entire azimuthal plane.

In this work, the uniform theory of diffraction with an imposed edge diffraction extension is utilized to analyze in detail the entire backscatter cross section of right, acute, and obtuse dihedral corner reflectors in the azimuthal plane for both the horizontal and vertical polarizations. All possible reflection–diffraction mechanisms of up to third order have been included in the analysis. Up to third-order terms are sufficient for the corner reflectors studied, but higher order mechanisms may be required for smaller interior angles. The total cross section is decomposed into individual components which explicitly show the dominant scattering mechanisms at specific orientations. Understanding how the total cross section is built from individual mechanisms is very important

Manuscript received March 21, 1986; revised May 15, 1987. This work was supported by the NASA Langley Research Center under Grant NAG-1-562 and by the Office of Naval Research through the ONR Graduate Fellowship Program.

The authors are with the Department of Electrical and Computer Engineering, Arizona State University, Tempe, AZ 85287.

IEEE Log Number 8716777.

0018-926X/87/1100-1235$01.00

for developing methods to reduce, enhance or synthesize particular backscatter characteristics of a particular target.

In addition, the problems associated with GTD (or UTD) in cross section analyses for targets formed of planar surfaces are presented. The UTD coefficients revert to Keller's original GTD forms as the distance of observation increases for the singly diffracted fields. The problems associated with the singularities of Keller's coefficients may be overcome if two mutually parallel edges exist on a planar surface, since the two singly diffracted fields together can produce finite cross sections. In this paper, it is shown that this cancellation will occur regardless of the GTD edge wedge parameters n, provided $1/n$ is noninteger on both edges. This property can be utilized in the analysis of a more general target by subdividing the target into rectangular segments which approximate the backscatter characteristics of the actual target. Sikta [11], [13] used this property in the subdivision of a polygonal plate into rectangular strips, but the subdivision can actually be used on more general solid objects for edges of noninteger $1/n$.

II. UTD Far-Field Analysis

The diffraction coefficients of the uniform theory of diffraction [2] have been used extensively in electromagnetic studies to add diffraction mechanisms to the geometrical optics reflected fields; however, these diffraction coefficients can become less convenient to use when applied to radar cross section analysis. In radar cross section analyses, the coefficients of the uniform theory of diffraction revert to the original GTD diffraction coefficients proposed by Keller [1] since the distance parameter for the singly diffracted fields is infinite. This occurs because the argument of the Fresnel transition function [2], $kLa^{\pm}(\psi \pm \psi_0)$, is large everywhere as $L \to \infty$ except for the infinitesimal angle surrounding the shadow boundaries where[1] $a^{\pm}(\psi \pm \psi_0) \to 0$. For large argument, the Fresnel transition function is nearly unity, and the UTD coefficients become identical to the original Keller coefficients. Unfortunately these original coefficients include singularities near incident and reflection shadow boundaries. For backscattering from a straight edge joining two planar surfaces, the shadow boundary singularity occurs at an aspect normal to either planar surface.

The total cross section for targets formed of planar surfaces will be finite whenever two associated parallel diffracting edges exist. Ross [7] showed that for the rectangular flat plate the diffraction coefficients for each edge were infinite near normal incidence but the singularities from each edge cancelled against each other to yield finite cross sections at all aspects for the singly diffracted field. This occurred because the edges of the rectangular plate are mutually parallel and the associated edge wedge angles are zero. Sikta [11], [13] used this property in his analysis of a general polygonal plate by subdividing each polygon into a number of rectangular strips to ensure continuity of the diffracted field near normal incidence.

It is shown in this paper that the diffracted field singularities will mutually cancel regardless of the edge wedge angles provided the edges are parallel. This is an important result because it allows the subdivision of a general solid object into rectangular segments, which are not necessarily flat rectangular strips, to ensure continuity of the backscatter cross section. The continuity is demonstrated using the Keller GTD diffraction coefficients. This continuity guarantees that when the dihedral corner reflector is analyzed using UTD, the cross section will be continuous (and relatively insensitive to distance) in the far field. However, if edges are not forced to occur in cancelling pairs, the UTD cross section will not be continuous and will be a function of distance. Indeed it will be unbounded near the reflection boundary, as the Keller GTD coefficients are. (The introduction of corner diffractions [11] can remove this restriction for flat plate structures, but not all of the corners on the dihedral corner reflector are of the type found on flat plates.)

To demonstrate the continuity of the fields from two mutually parallel edges, let us refer to the geometry of a plate of width w, displayed in Fig. 1. The two edges, characterized by the arbitrary wedge parameters n_1 and n_2, diffract an incident wave toward the backscatter direction $\phi = \psi_1 = \pi - \psi_2$. The incident field can be written as

$$E^i = E_0 e^{+jk(x\cos\phi + y\sin\phi)} \tag{1}$$

where its polarization is either soft or hard.

The total diffracted field for the soft or the hard polarization is

$$\begin{aligned} E_{s,h}(s) &= E_{s,h}^{d_1}(s) + E_{s,h}^{d_2}(s) \\ &= \left\{E_0 \frac{e^{-jks}}{\sqrt{s}}\right\} [D_{s,h}(\psi_1, \psi_1, n_1) e^{-jkw\cos\psi_1} \\ &\quad + D_{s,h}(\psi_2, \psi_2, n_2) e^{+jkw\cos\psi_1}] \end{aligned} \tag{2}$$

where

$$D_{s,h}(\psi, \psi, n) = \frac{e^{-j\pi/4}\sin\frac{\pi}{n}}{n\sqrt{2\pi k}} \cdot \left[\frac{1}{\cos\left(\frac{\pi}{n}\right) - 1} \mp \frac{1}{\cos\left(\frac{\pi}{n}\right) - \cos\left(\frac{2\psi}{n}\right)}\right]. \tag{3}$$

The difficulties occur in both diffraction coefficients when $\psi = \pi/2$ (normal incidence).

The total field can be expressed as

$$E_{s,h}(s) = \left\{E_0 \frac{e^{-jks}}{\sqrt{s}}\right\} \left[\frac{e^{-j\pi/4}}{\sqrt{2\pi k}}\right] [\mathfrak{D}_a \mp \mathfrak{D}_b] \tag{4}$$

where the upper sign is chosen for soft polarization and the lower sign is chosen for hard polarization. The functions $\mathfrak{D}_a$ and $\mathfrak{D}_b$ are given by

$$\mathfrak{D}_a = \frac{\frac{1}{n_1}\sin\frac{\pi}{n_1}}{\cos\left(\frac{\pi}{n_1}\right) - 1} e^{-jkw\cos\phi} + \frac{\frac{1}{n_2}\sin\frac{\pi}{n_2}}{\cos\left(\frac{\pi}{n_2}\right) - 1} e^{+jkw\cos\phi} \tag{5}$$

[1]The diffraction directions ϕ and ϕ' of [2] are referred to here as ψ and ψ_0, respectively, as in [5]. In this paper, ϕ is the azimuthal angle in the spherical and cylindrical coordinate systems.

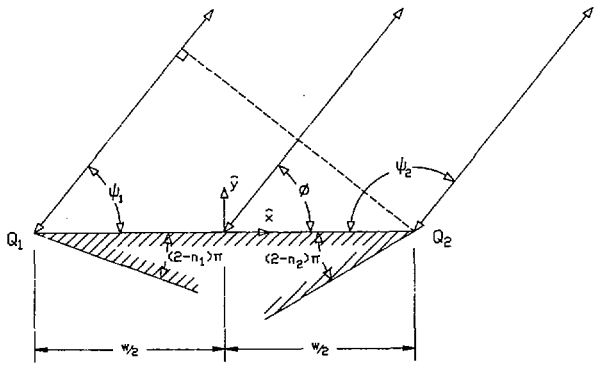

Fig. 1. A flat conducting surface with parallel edges of arbitrary wedge angles.

$$\mathfrak{D}_b = \frac{\frac{1}{n_1}\sin\frac{\pi}{n_1}\left(e^{-jkw\cos\phi}\right)}{\cos\left(\frac{\pi}{n_1}\right)-\cos\left(\frac{2\phi}{n_1}\right)} + \frac{\frac{1}{n_2}\sin\frac{\pi}{n_2}\left(e^{+jkw\cos\phi}\right)}{\cos\left(\frac{\pi}{n_2}\right)-\cos\left(\frac{2\pi-2\phi}{n_2}\right)}. \quad (6)$$

At $\phi = \pi/2$, $\mathfrak{D}_a$ is continuous and is given by

$$\mathfrak{D}_a = \frac{\frac{1}{n_1}\sin\frac{\pi}{n_1}}{\cos\left(\frac{\pi}{n_1}\right)-1} + \frac{\frac{1}{n_2}\sin\frac{\pi}{n_2}}{\cos\left(\frac{\pi}{n_2}\right)-1}. \quad (7)$$

However, both terms in the expression for $\mathfrak{D}_b$ are infinite at $\phi = \pi/2$. Adding over a common denominator, $\mathfrak{D}_b = f_1/f_2$, and using L'Hôpital's rule for indeterminate ratios,

$$\mathfrak{D}_b\Big|_{\phi=\pi/2} = \frac{f_1''}{f_2''}\Big|_{\phi=\pi/2} \quad (8)$$

where

$$f_1''\Big|_{\phi=\pi/2} = \frac{d^2 f_1}{d\phi^2}\Big|_{\phi=\pi/2} = (-j8kw)\left(\frac{1}{n_1}\sin\frac{\pi}{n_1}\right)\left(\frac{1}{n_2}\sin\frac{\pi}{n_2}\right) + \frac{4}{n_2}\left(\frac{1}{n_1}\sin\frac{\pi}{n_1}\right)\left(\frac{1}{n_2}\cos\frac{\pi}{n_2}\right) + \frac{4}{n_1}\left(\frac{1}{n_2}\sin\frac{\pi}{n_2}\right)\left(\frac{1}{n_1}\cos\frac{\pi}{n_1}\right) \quad (9)$$

$$f_2''\Big|_{\phi=\pi/2} = \frac{d^2 f_2}{d\phi^2}\Big|_{\phi=\pi/2} = -8\left(\frac{1}{n_1}\sin\frac{\pi}{n_1}\right)\left(\frac{1}{n_2}\sin\frac{\pi}{n_2}\right). \quad (10)$$

The result for the diffracted fields from a flat surface at normal incidence, for the soft or hard polarization, is

$$E_{s,h}(s)\big|_{\phi=\pi/2} = E_0\frac{e^{-jks}}{\sqrt{s}}\left[\frac{e^{-j\pi/4}}{\sqrt{2\pi k}}\right][\mathfrak{D}_a \mp \mathfrak{D}_b] \quad (11)$$

where $\mathfrak{D}_a$ is given by (7) and $\mathfrak{D}_b$ is given by (8)–(10). If $1/n_1$ and $1/n_2$ are not integers, the total field given in (11) will be finite at all aspects provided both edges are visible.

It is permissible then to use the UTD coefficients at both near and far observation distances, with the far-field limit being the cross section of interest. For a target formed of flat surfaces with mutually parallel edges, the UTD cross section will be nearly invariant with distance provided the distance is large. The cross section of individual singly reflected fields or singly diffracted fields increases as the distance increases, however the total cross section approaches a finite value. The "far-field" criterion [18] can be used as a measure of the minimum distance required for accurate results.

Although the diffracted field from a pair of parallel edges is continuous, cases may exist where both edges of a plate may not be visible near normal incidence. This normally occurs because another unrelated object passes in the line of sight from the target to the radar. Such is the case, for example, for the dihedral corner reflector when one plate obstructs the view of one of the edges of the second plate. Clearly in cases such as these, there is only one edge diffraction, and the field is no longer continuous near normal incidence.

Geometrically, under these circumstances, one portion of the plate is illuminated while another portion is shadowed. An abrupt discontinuity in the GO field incident upon the plate is created because of the shadow cast by the obstructing object. Since abrupt discontinuities must not exist, some diffraction mechanism should be introduced to assure continuity in the radar cross section pattern [10]. In the analysis of the dihedral corner reflector, an edge diffraction has been imposed exactly at the shadow edge to remove the discontinuity in the cross section pattern. The choice of using an edge at this position is not a rigorous use of the UTD, but is a judicious choice which gives the same contribution from the visible surface as a physical optics solution [17]. No other UTD mechanisms, in a strict application, cancel the singularity due to the one solitary visible edge. The edge position is a function of the dihedral orientation since the shadow edge moves as the dihedral corner reflector is rotated. The imposed edge diffraction was included if the aspect was such that the incident field was nearly normal to one of the two flat plates, and if at the same orientation, the second plate cast a shadow across the first. The appropriate choice of edge parameter n is not apparent for this imposed edge so some discretion is allowed. Since only a half plane is illuminated, it seems appropriate to select an equivalent edge which has only one face illuminated; that is an edge with included angle in the range of $0° < \mathrm{WA} < 90°$. Since the resulting cross section is relatively insensitive to the choice of WA, a wedge angle of $0°$ was chosen; that is, $n = 2$ for the imposed edge.

The aforementioned concepts are incorporated in the UTD analysis of dihedral corner reflectors discussed next.

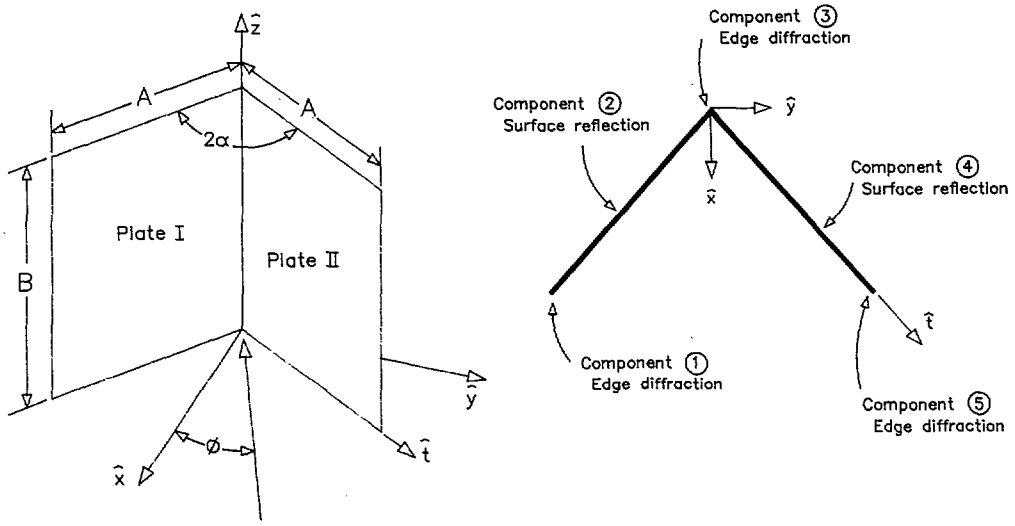

Fig. 2. Dihedral corner reflector geometry and backscatter nomenclature.

III. UTD Analysis of Dihedral Corner Reflectors

The usefulness and accuracy of the uniform theory of diffraction is evaluated through the study of the dihedral corner reflector shown in Fig. 2. This corner reflector is comprised of two rectangular flat conducting plates which are joined along an edge, forming an interior angle of 2α. The dihedral corner reflector is oriented such that its vertex is along the z-axis and the bottom edges lie in the x-y plane. The monostatic radar cross section is computed analytically in the azimuthal plane where $\theta = 90°$ and $0° \leq \phi \leq 360°$. The two cases of vertical and horizontal polarization are considered, where the vertically polarized radar cross section is determined using the components of the incident and scattered electric fields which are parallel to the z-axis, and the horizontally polarized radar cross section is determined using the components of the incident and scattered electric fields which are perpendicular to the z-axis.

The technique utilized to find the backscattered fields from the dihedral corner reflector begins by considering the dihedral to be a truncated two-dimensional object, which is illuminated by an incident cylindrical wave. If the radar cross section per unit length of the corresponding two-dimensional dihedral corner reflector is known, the three-dimensional radar cross section of the truncated dihedral corner reflector can be obtained by [7], [9], [19]

$$\sigma = \frac{8L^2}{\lambda}\sigma_1 \tag{12}$$

where σ is the three-dimensional radar cross section of the truncated two-dimensional object, σ_1 is the two-dimensional radar cross section of the corresponding two-dimensional object, L is the length of the truncated object, and λ is the free-space wavelength.

It is necessary to develop some strategy for naming scattering mechanisms from both geometrical optics and geometrical diffraction. Toward meeting this requirement, a naming convention has been developed in which each edge diffraction and each surface reflection is assigned a unique number. The numbering scheme, depicted in Fig. 2, is as follows:

1) the diffraction from the exterior edge of plate I
2) the reflection from the surface of plate I
3) the diffraction from the edge where plate I joins plate II
4) the reflection from the surface of plate II
5) the diffraction from the exterior edge of plate II.

With this notation, every possible component of the backscattered field can be assigned a unique number describing the sequence of reflections and diffractions. The component is specified by a coalescence of the digits of the individual scattering mechanisms. The notation adopted here is to precede each component by a capital letter C to identify the digits as the description of a component of the backscattered field. The order of the digits defines the order of occurrence of the individual reflections and diffractions. As an example, the notation C251 uniquely defines the component of the total backscattered field which is due to reflection from plate I (2), followed by diffraction from the outside edge of plate II (5), and diffraction from the outside edge of plate I (1). The final diffraction direction is toward the original direction of incidence for the monostatic case. Some typical scattering mechanisms are shown in Fig. 3.

Using the described notation, the total backscattered field is found as a summation of the following terms

- Components due to single reflections:

  * C2 C4.

- Components due to single diffractions:

  * C1 C3 C5.

- Components due to double reflections:

  * C24 C42.

- Components due to one reflection and one diffraction:

  * C14 C41 C25 C52.

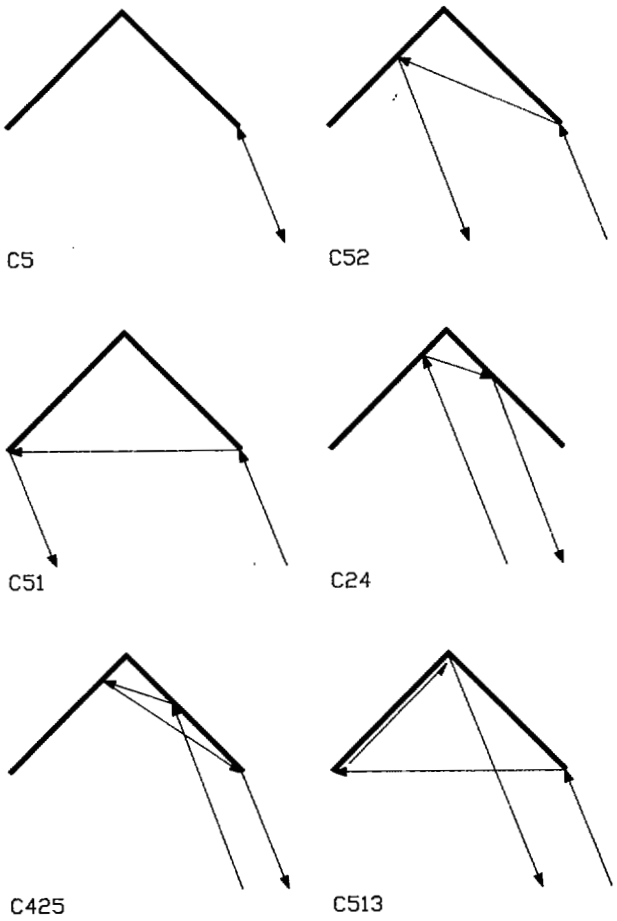

Fig. 3. Examples of components of the UTD backscattered field.

- Components due to two diffractions:

  * C13 C31 C53 C35 C15 C51.

- Components due to three reflections:

  * C242 C424.

- Components due to two reflections and one diffraction:

  * C252 C414 C142 C241 C524 C425.

- Components due to one reflection and two diffractions:

  * C141 C525 C152 C251 C514 C415
  * C253 C352 C413 C314.

- Components due to three diffractions:

  * C131 C535 C135 C531 C153 C351
  * C513 C315 C151 C515 C313 C353.

- Components due to imposed edges:

  * $C2_{im}$ $C4_{im}$.

All these components are included in the analysis presented in this paper when determining the backscatter cross section for the dihedral corner reflector. While this is a complete third-order analysis, higher than third-order terms become necessary as the dihedral angle decreases. For the vertically polarized case, the components which include multiple diffraction between two edges of the same plate will vanish due to the nature of the diffraction coefficients, which impose the electromagnetic boundary condition that tangential electric fields on a perfect conductor are identically zero. These components are nonzero if the slope diffraction coefficients [20] of UTD are utilized.

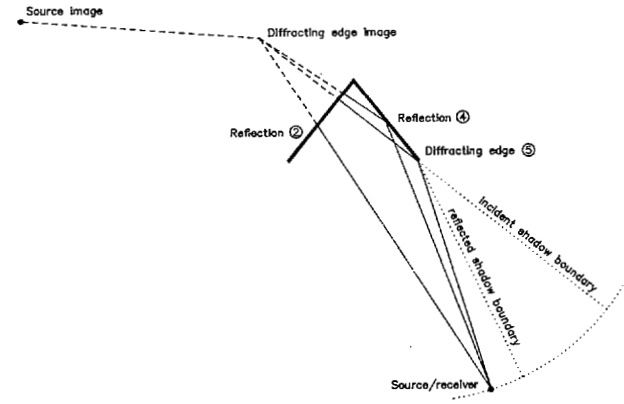

Fig. 4. Components of the UTD backscattered field which guarantee continuity across the reflection shadow boundary.

Many of the terms in this listing are reciprocal because the ordering of the digits is symmetric. For example C425 and C524 are equivalent, C25 and C52 are equivalent, and so on. Other terms such as C525 are their own reciprocal because of the symmetry in the sequence of diffractions and reflections. Fig. 4 illustrates the need to include C525 to obtain continuity in the fields due to C425 and C25, as well as in the reciprocal fields C524 and C52. In this figure, the fields at the image of edge 5 are due to the "direct" path C25, the "reflected" path C425, and the "diffracted" path C525, and all three terms are required for continuity of the field at the source image. Similarly, in the reciprocal direction, the fields at the receiver due to diffraction at the image of edge 5 follow a "direct" path C52, a "reflected" path C524, and a "diffracted" path C525, to the receiver and again all three terms are needed to assure continuity.

In the cross section analysis, the method of images is utilized extensively. In the cylindrical coordinate system, as shown in Fig. 2, the source and all subsequent images for the dihedral corner reflector lie in the x-y plane. The location of the source, diffraction points, and all images of the source can be tabulated in cylindrical coordinates using the geometry shown. Here R represents the distance from the source to the vertex of the dihedral corner, and A is the width of the plates of the dihedral corner reflector. The locations of the source, images, and diffraction points are given in a cylindrical coordinate system (ρ, ϕ) as

- the source location: $P = (R, \phi)$
- the point of diffraction on edge 1: $P_1 = (A, 2\pi - \alpha)$
- the point of diffraction on edge 5: $P_5 = (A, \alpha)$
- the point of diffraction on edge 3: $P_3 = (0, 0)$
- the image of the source through surface 2: $P_2 = (R, 2\pi - 2\alpha - \phi)$
- the image of the source through surface 4: $P_4 = (R, 2\alpha - \phi)$

- the image of P_2 through surface 4: $P_{24} = (R, 4\alpha + \phi - 4\pi)$
- the image of P_4 through surface 2: $P_{42} = (R, 2\pi - 4\alpha + \phi)$
- the image of P_1 through surface 4: $P_{14} = (A, 3\alpha)$
- the image of P_5 through surface 2: $P_{52} = (A, 2\pi - 3\alpha)$
- the location of the imposed edge on surface 2:

$$P_{2,\text{im}} = \left[\frac{A^2 - R^2}{2A \cos 2\alpha - 2R \cos (\alpha + \phi)}, 2\pi - \alpha \right]$$

- the location of the imposed edge on surface 4:

$$P_{4,\text{im}} = \left[\frac{A^2 - R^2}{2A \cos 2\alpha - 2R \cos (2\pi - \phi - \alpha)}, \alpha \right].$$

The amplitude and phase of the diffracted and reflected waves depend upon the distance of wave travel between scattering points. If any two points P_a and P_b are given in terms of their cylindrical coordinates, then the distance of wave travel s, between P_a and P_b, can be found by

$$s = [\rho_a^2 + \rho_b^2 - 2\rho_a\rho_b \cos (\phi_a - \phi_b) + (z_a - z_b)^2]^{1/2}. \quad (13)$$

In the two-dimensional analysis, z_a and z_b are zero.

For a given reflection to exist, the ray from a source image or diffraction edge image must pass through the reflecting plate. If the originating point is given in terms of its rectangular coordinates in the x-y plane as (x_a, y_a), and if the terminating point is given in terms of its rectangular coordinates in the x-y plane as (x_b, y_b), then the ray through the two points is given as

$$y = \left[\frac{y_b - y_a}{x_b - x_a} \right] x + \left[\frac{y_a x_b - y_b x_a}{x_b - x_a} \right]. \quad (14)$$

A point on the plates of the reflector, in the x-y plane can be given in terms of its cylindrical coordinates as (ρ, ϕ) where $\phi = 2\pi - \alpha$ on plate I and $\phi = \alpha$ on plate II. The radial distance of the intersection of the ray and the plate is then

$$\rho = \frac{y_a x_b - y_b x_a}{(y_b - y_a) \cos \phi - (x_b - x_a) \sin \phi}. \quad (15)$$

The reflection exists if ρ lies in the range $0 < \rho < A$ where A is the width of the dihedral plates. The equation has no solution if $\tan \phi = (y_b - y_a)/(x_b - x_a)$ and hence no reflection will exist.

For any reflection–diffraction sequence which begins or ends with a reflection, the reflection surface must also be visible to the source and observation points. For the monostatic cross section of the dihedral corner, the plates are visible or partially visible at certain aspects.

For reflection 2, the surface is

- entirely visible if $0 < \phi < \alpha$ or $\pi - \alpha < \phi < 2\pi$
- not visible if $\cos^{-1} [(A \cos \alpha)/R] < \phi < \pi - \alpha$
- partially visible elsewhere.

The visible portion of the plate is given by

$$A \frac{\sin (\phi - \alpha)}{\sin (\phi + \alpha)} \le \rho \le A. \quad (16)$$

For reflection 4, the surface is

- entirely visible if $0 < \phi < \pi + \alpha$ or $2\pi - \alpha < \phi < 2\pi$
- not visible if $\pi + \alpha < \phi < 2\pi - \cos^{-1} [(A \cos \alpha)/R]$
- partially visible elsewhere.

The visible portion of the plate is given by

$$A \frac{\sin (\phi + \alpha)}{\sin (\phi - \alpha)} \le \rho \le A. \quad (17)$$

A reflection–diffraction sequence which begins or ends with a diffraction will exist if the diffracting edge is visible from the source and observation point. For the dihedral corner reflector

- edge 1 is visible if

$$0 < \alpha < \cos^{-1} \left[\frac{A \cos \alpha}{R} \right] \text{ or } \pi - \alpha < \phi < 2\pi; \quad (18)$$

- edge 3 is visible if

$$0 < \phi < \alpha \text{ or } 2\pi - \alpha < \phi < 2\pi \quad \text{(interior corner)}$$
$$\alpha < \phi < 2\pi - \alpha \quad \text{(exterior corner)}; \quad (19)$$

- edge 5 is visible if

$$0 < \phi < \pi + \alpha \text{ or } 2\pi - \cos^{-1} \left[\frac{A \cos \alpha}{R} \right] < \phi < 2\pi. \quad (20)$$

Locating the originating or terminating point by its rectangular coordinates in the x-y plane (x_a, y_a), the diffraction angles, ψ_0 and ψ, can be found

- on edge 1 as

$$\psi_1 = \pi + \alpha + \tan^{-1} \left[\frac{y_a - y_1}{x_a - x_1} \right]; \quad (21)$$

- on edge 3, for interior diffraction as

$$\psi_{3i} = \alpha + \tan^{-1} \left[\frac{y_a - y_3}{x_a - x_3} \right]; \quad (22)$$

- on edge 3, for exterior diffraction as

$$\psi_{3e} = -\alpha + \tan^{-1} \left[\frac{y_a - y_3}{x_a - x_3} \right]; \quad (23)$$

- on edge 5 as

$$\psi_5 = -\alpha + \tan^{-1} \left[\frac{y_a - y_5}{x_a - x_5} \right]; \quad (24)$$

- on the imposed edge on surface 2 as

$$\psi_{2,\text{im}} = \alpha + \tan^{-1} \left[\frac{y_a - y_{2,\text{im}}}{x_a - x_{2,\text{im}}} \right]; \quad (25)$$

- on the imposed edge on surface 4 as

$$\psi_{4,\text{im}} = -\alpha + \tan^{-1} \left[\frac{y_a - y_{4,\text{im}}}{x_a - x_{4,\text{im}}} \right]; \quad (26)$$

where ψ_1, ψ_{3i}, ψ_{3e}, ψ_5, $\psi_{2,\text{im}}$, or $\psi_{4,\text{im}}$ can represent either ψ or ψ_0 for a given diffraction, and where (x_j, y_j) are the coordinates of the diffracting edge. In these expressions, particular attention must be paid to the inverse tangent function to assure that the angles ψ and ψ_0 lie in the appropriate quandrants and to satisfy $0 \leq \psi \leq n\pi$ and $0 \leq \psi_0 \leq n\pi$. Equations (21)–(26) should not be simplified by using the "far-field" approximation in which all diffracted rays are considered to be parallel to the radial direction. The UTD diffraction coefficients are extremely sensitive to ψ and ψ_0 near shadow boundaries for large distances of observation, and approximations of the angles leads to large discontinuities in the cross section patterns. The common technique of considering all diffracted rays to be parallel to each other is too gross of an approximation for determining these angles at large distances. The "far-field" approximation could, of course, be used with Keller's coefficients at an infinite distance as in Section II and as Ross [7] has done for the flat rectangular plate by requiring the diffractions from the edges to lie on opposite sides of the respective shadow boundaries.

The reflected fields for the dihedral corner reflector are found using image theory with the image locations tabulated previously. The field due to a source or image for the two-dimensional geometry is

$$\bar{E} = \pm \hat{a}_z E_0 \frac{e^{-jks}}{\sqrt{s}}, \quad \text{(for vertical polarization)} \qquad (27)$$

$$\bar{H} = \hat{a}_z H_0 \frac{e^{-jks}}{\sqrt{s}}, \quad \text{(for horizontal polarization)} \qquad (28)$$

where the upper sign is used for an even number of reflections and the lower sign is used for an odd number of reflections for the vertical polarization. The distance s between the source image and the observation point is found using (13).

The diffracted fields for the dihedral corner reflector are found using the UTD coefficients of [2]. The field is a product of the diffraction coefficients for each edge and the associated spreading factors. The diffracted field is

$$\bar{E} = \hat{a}_z E_0 \frac{e^{-jks_1'}}{\sqrt{s_1'}} \prod_{i=1}^{N} D_s(L_i, \psi_i, \psi_{0i}, n_i) \frac{e^{-jks_i}}{\sqrt{s_i}},$$

(for vertical polarization) (29)

$$\bar{H} = \hat{a}_z H_0 \frac{e^{-jks_1'}}{\sqrt{s_1'}} \prod_{i=1}^{N} D_h(L_i, \psi_i, \psi_{0i}, n_i) \frac{e^{-jks_i}}{\sqrt{s_i}},$$

(for horizontal polarization) (30)

where N is the number of diffractions and ψ_i, ψ_{0i} and n_i are the diffraction parameters associated with diffraction i, and $L_i = (s_i s_i')/(s_i + s_i')$. The distance s_i' is measured from the source to the diffracting edge, while the distance s_i is measured from the diffracting edge to the next edge or to the observation point. The reflected–diffracted fields are found from the same expression with the appropriate image used for each reflection and with (29) multiplied by $(-1)^{N_r}$ where N_r is the number of reflections. The locations of all the images and all the angles ψ_i and ψ_{0i} have been presented here.

Using the product of diffraction terms, as in (29) and (30), is a simple method for determining the double and triple diffracted fields and good results are obtained away from the forward scattering transition regions. Near these transition regions, the diffracted field is not a ray type field and improved results can be obtained by utilizing improved asymptotic formulations [21]–[24]. Because of the large number of terms involved in the analysis of the dihedral corner reflector, these refinements in individual components near the transitional regions were not included in determining the total cross section pattern.

IV. Comparison with Experimental Results

The specific dihedral corner reflectors, for which limited experimental results were available, were constructed of two square plates each with sides of 5.6088 λ. These experimental measurements, reported in [25], were conducted at 9.4 GHz using vertically polarized fields (i.e., the electric field vector was parallel to the longitudinal axis of the dihedral corner reflector). The backscatter cross sections, as a function of azimuthal angle in a plane perpendicular to the dihedral corner reflector longitudinal axis, were available for reflectors with 90°, 98°, and 77° interior angles.

One of the advantages of analyzing target backscatter using UTD is that the contributions of different mechanisms can be separated so that the effect of each structural element in the target can be identified. In Figs. 5 and 6, the backscatter cross section components for vertical and horizontal polarizations are illustrated for different reflection and diffraction mechanisms as a function of the observation direction ϕ. The total radar cross section (RCS) is subdivided into groups of individual components and the radar cross section due to each group is shown separately. Each figure contains 12 graphs, and each graph shows the radar cross section of one or two particular groups. The subdivision usually combines only the symmetric or reciprocal components. For example, graph 1 shows the backscatter cross section when only components C2 and C4 are considered, where C2 and C4 are the single specular reflection components from the dihedral plates. Graph 5 illustrates the component due to the imposed edges on surfaces 2 and 4. Graph 11 shows the cross section due solely to all the third-order diffractions which include diffraction from the vertex of the dihedral (edge 3). Since slope diffraction coefficients have not been considered, these third-order terms are all identically zero for the vertically polarized case. However, these and other higher order diffraction terms are nonzero for the horizontal polarization, and they tend to result in RCS patterns with higher sidelobes. The final graph, numbered 12, shows the total cross section as the sum of all individual components up to third-order mechanisms. The form of the individual components would be altered if slope diffractions [20] or asymptotic extensions of the UTD [21]–[24] were included. Although some of the individual terms are very small for the 90° dihedral corner reflector, these same terms may become dominant for the obtuse or acute corner

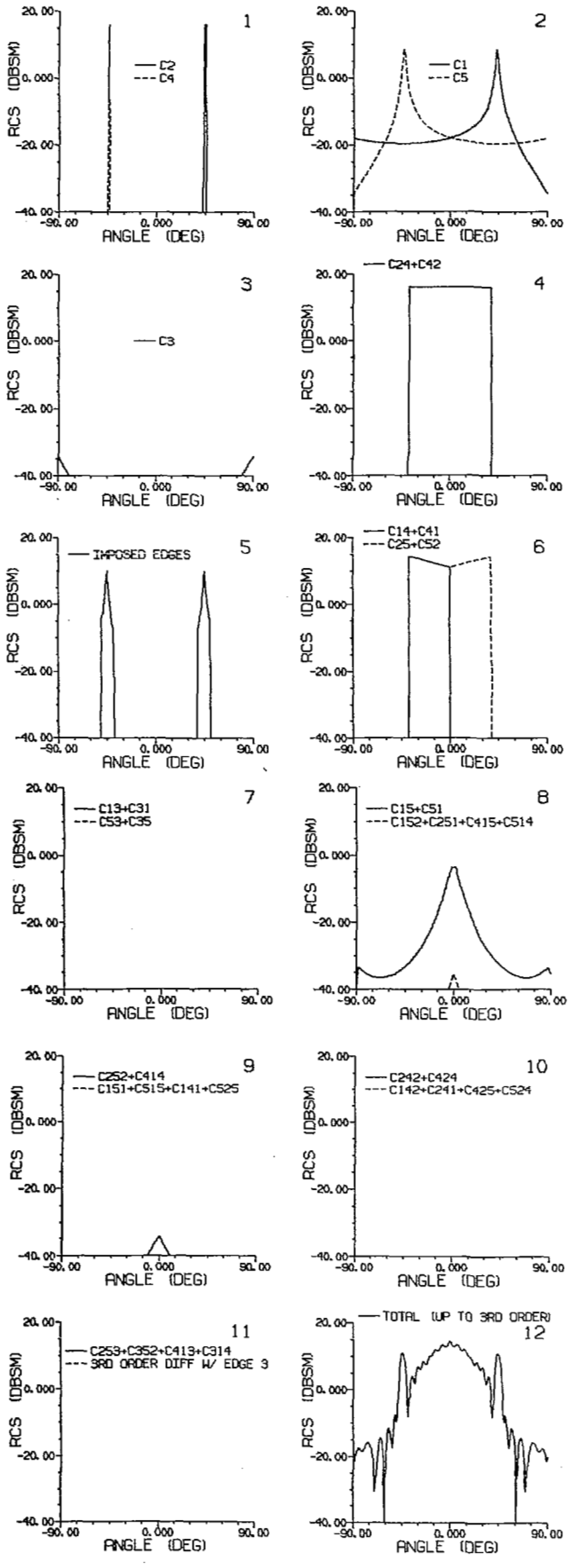

Fig. 5. Components of the radar cross section of a 90° dihedral corner reflector using UTD ($A = B = 5.6088\ \lambda$, vertical polarization, $f = 9.4$ GHz, $R = 200\ \lambda$).

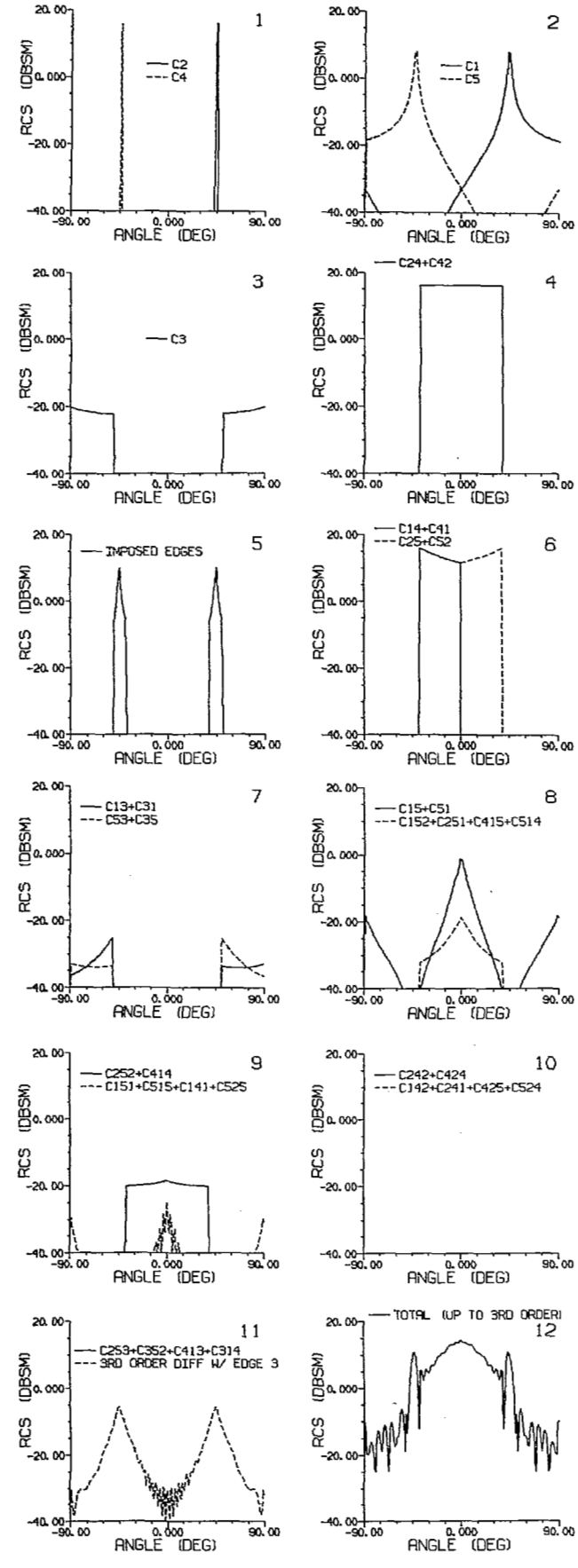

Fig. 6. Components of the radar cross section of a 90° dihedral corner reflector using UTD ($A = B = 5.6088\ \lambda$, horizontal polarization, $f = 9.4$ GHz, $R = 200\ \lambda$).

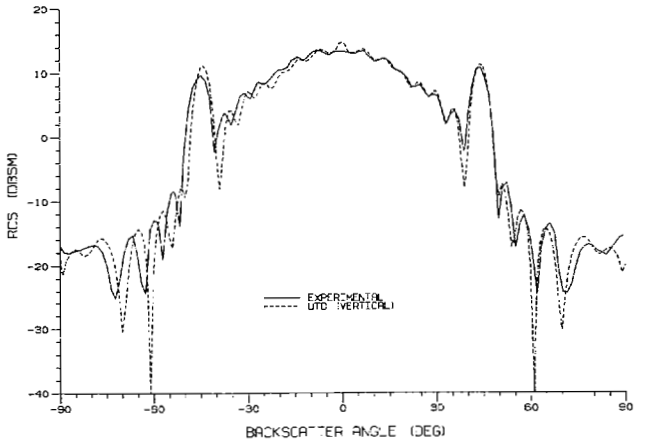

Fig. 7. Experimental and UTD cross sections of the 90° dihedral corner reflector ($A = B = 5.6088$ λ, $f = 9.4$ GHz, $R = 200$ λ).

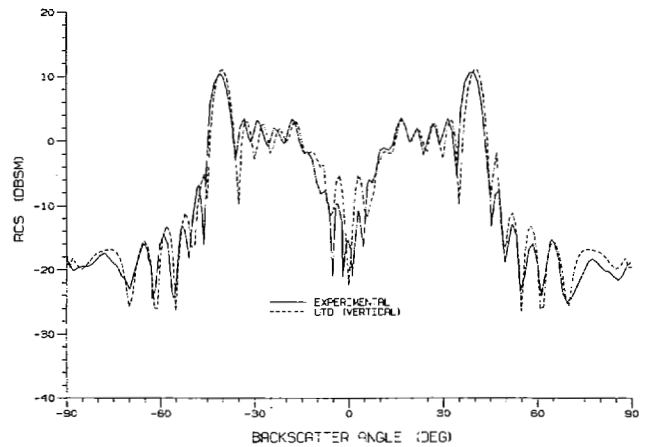

Fig. 8. Experimental and UTD cross sections of the 98° dihedral corner reflector ($A = B = 5.6088$ λ, $f = 9.4$ GHz, $R = 200$ λ).

reflector [14]. Hence, to attain good accuracy, no terms should be ignored.

In Figs. 7, 8 and 9, the vertically polarized radar cross section patterns of the dihedral corner reflectors found using UTD are compared with measured data for the 90°, 98°, and 77° corner reflectors. The distance of observation was 200 λ for these calculations to satisfy the far-field criterion, and the cross section is relatively independent of distance for larger distances. The RCS must be independent of distance for it to be a useful parameter in the radar range equation, since the basic motivation behind introducing cross sections as target parameters is to separate the effects of radar distance and configuration from the target specification. The UTD analytical results compare extremely well with the experimental data as the curves match many of the major and minor lobe structures of the measured cross sections. While the UTD predicted patterns are symmetric about $\phi = 0°$, the measured data are not necessarily symmetric, especially near minor lobes. For this reason, the two cross sections may agree better on one side than on the other. Achieving perfectly symmetric measured cross sections, especially at low levels, is an extremely demanding task.

To examine the influence of polarization on the RCS patterns of dihedral corner reflectors, computations were also made assuming horizontal polarization for right, obtuse, and acute corner reflectors. The results are shown in Figs. 10, 11, and 12 where they are compared with the corresponding ones for vertical polarization. While many of the multiple edge-to-edge diffraction terms for the vertical polarization are zero, they are nonzero and become more important for the horizontal polarization. Because of this effect, the horizontal polarization RCS patterns for all three corner reflectors examined here tend to exhibit higher sidelobes. The cross section pattern for the 77° dihedral corner reflector is altered dramatically by the change in polarization. In the forward region for this corner reflector, the vertically polarized cross section tends to be larger than the horizontal case. The null at $\phi = 0°$ in the 98° corner reflector cross section pattern for vertical polarization is noticeably absent for the horizontal polarization. In the azimuthal plane, the UTD theory used here predicts no cross-polarized components for the dihedral corner reflector backscatter for either polarization. This occurs because the analysis is based on a two-dimensional geometry which has no cross-polarized return.

The radar cross sections determined using UTD have been extended to the back side of the dihedral corner reflector so that the entire 360° azimuthal plane may be examined. Although the dihedral corner reflector is commonly used in the forward region only, where the double reflections are dominant, exterior corners will exist on more complex structures such as ships, aircraft or other objects. The cross section in the back region is compared for the horizontal and vertical polarizations for a 90° corner reflector in Fig. 13. Again the horizontal polarization cross section tends to have larger sidelobes, although the major lobes are nearly identical.

Small angular misalignments in the lobe structures in Figs. 7–13 will occur whenever the UTD cross section is evaluated at a finite distance. A major lobe should occur at $\phi = 135°$ in the cross section pattern of Fig. 13, but occurs at $\phi = 134.2°$ using UTD at a distance of 200 λ. The angular error can be reduced by choosing a larger distance for the UTD analysis; however, higher precision would then be necessary when determining the UTD diffraction coefficients. The coefficients become very sensitive to angular inaccuracies near shadow boundaries as the distance of observation increases.

V. Conclusion

The uniform theory of diffraction plus an imposed edge extension has been used to predict the radar cross section of dihedral corner reflectors, and the analytical results were shown to agree extremely well with experimental data over a wide range of aspect angles. UTD is able to predict many of the fine details of the dihedral radar cross section pattern, even near the minor lobes, when third-order reflection–diffraction mechanisms are included. The total cross section is constructed from many different mechanisms, and each mechanism can become important for a given polarization, orientation, or interior angle. Therefore to achieve good accuracy, these higher order terms must not be ignored.

In the forward region, the choice of polarization has only a minor effect on the RCS of the 90° corner reflector. For the 98° corner reflector, a deep null at $\phi = 0°$ is present for

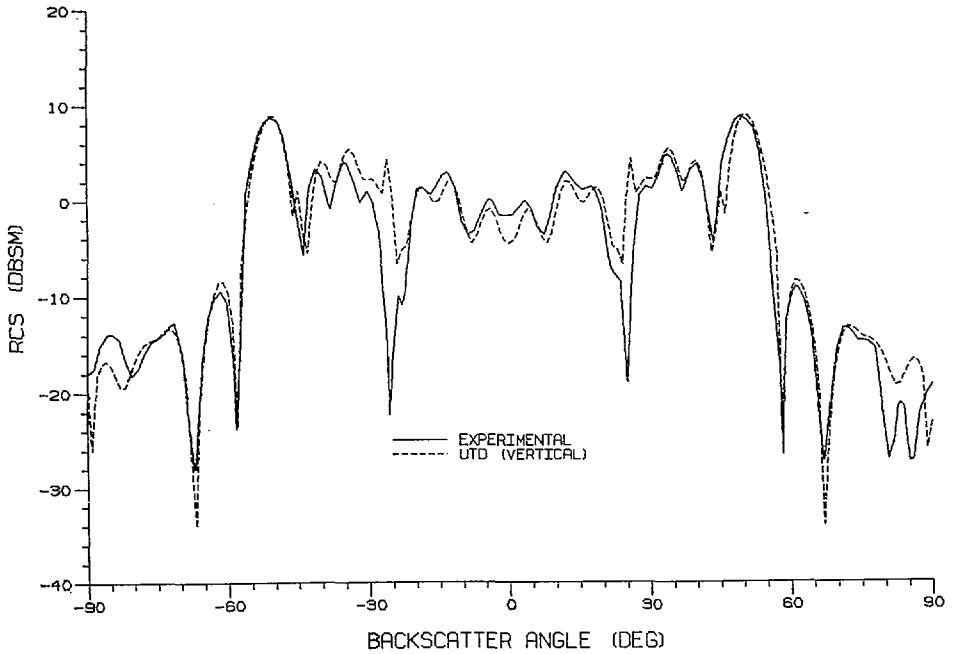

Fig. 9. Experimental and UTD cross sections of the 77° dihedral corner reflector ($A = B = 5.6088\ \lambda$, $f = 9.4$ GHz, $R = 200\ \lambda$).

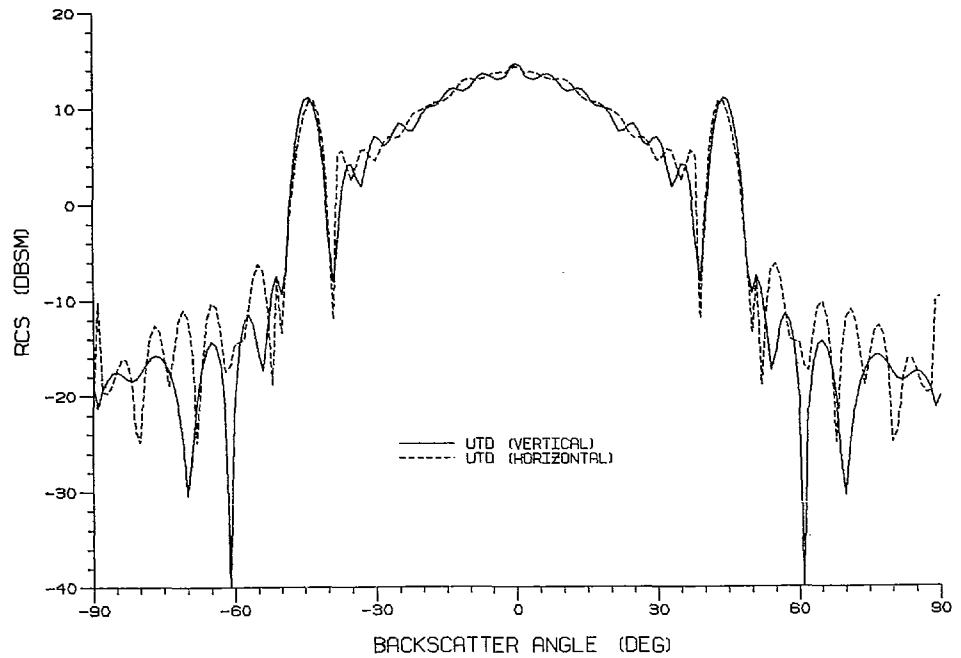

Fig. 10. UTD cross sections of the 90° dihedral corner reflector ($A = B = 5.6088\ \lambda$, $f = 9.4$ GHz, $R = 200\ \lambda$).

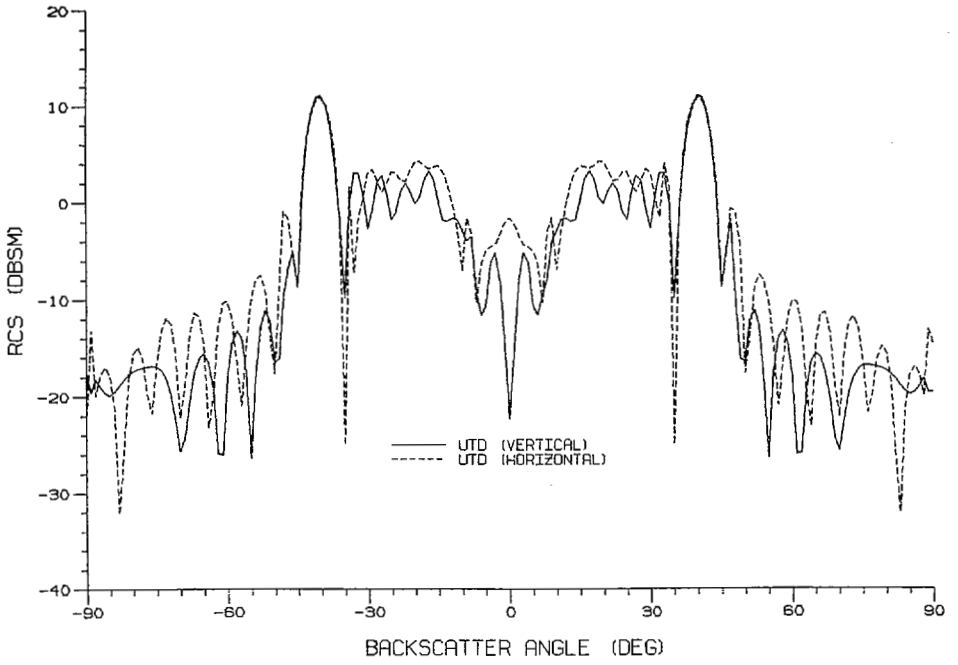

Fig. 11. UTD cross sections of the 98° dihedral corner reflector ($A = B =$ 5.6088 λ, $f = 9.4$ GHz, $R = 200$ λ).

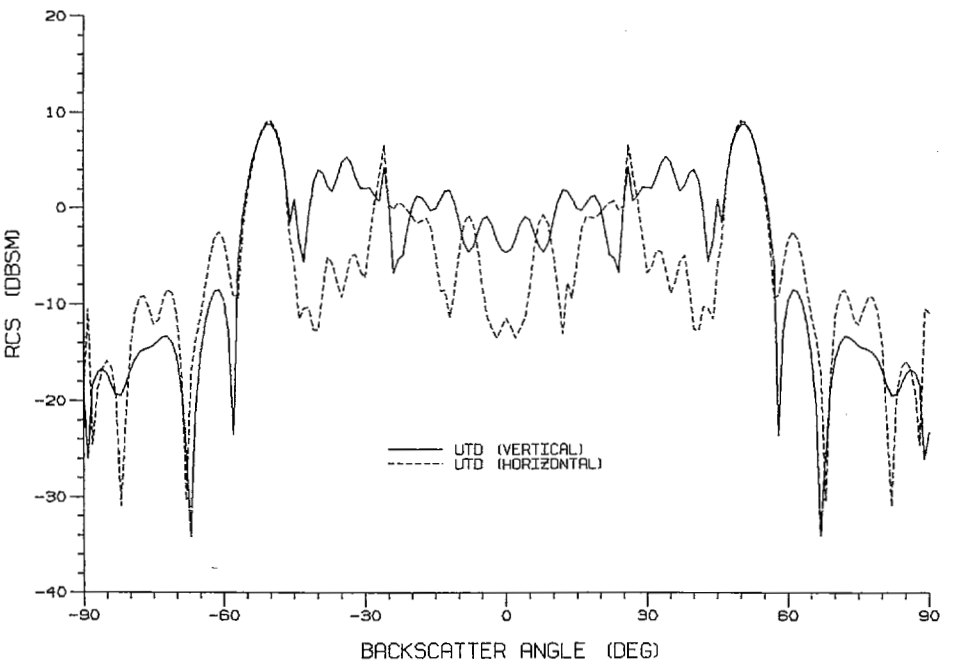

Fig. 12. UTD cross sections of the 77° dihedral corner reflector ($A = B =$ 5.6088 λ, $f = 9.4$ GHz, $R = 200$ λ).

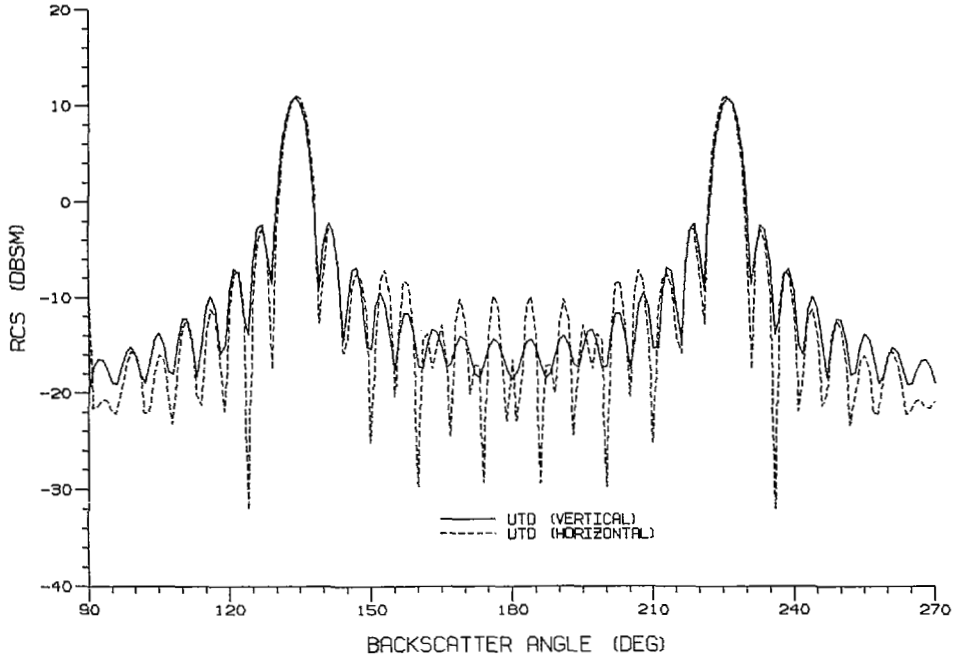

Fig. 13. UTD cross sections of the backside of the 90° dihedral corner reflector ($A = B = 5.6088\ \lambda$, $f = 9.4$ GHz, $R = 200\ \lambda$).

vertical polarization but is absent for horizontal polarization. Effects such as this can be used as tools to design low RCS surfaces. For the 77° dihedral corner reflector, the radar cross sections for the principle polarizations are markedly different, with the horizontal RCS generally exhibiting lower levels in this region. However, for all three corner reflectors, the horizontally polarized patterns tend to have higher sidelobes. In all reflectors considered, the UTD theory predicts no cross-polarized components in the azimuthal plane for either polarization because the analysis is based on a two-dimensional geometry.

For a planar reflecting surface, the singly diffracted fields of the UTD were shown to become infinite as the aspect direction nears the normal to the flat surface. It has been shown here that the sum of the diffracted fields will be finite as normal incidence is approached, provided that two mutually parallel edges exist which are perpendicular to the plane of observation.

The far-field approximation can be utilized for determining the amplitude spreading factor and phase factor for diffracted rays, but it should not be used to determine the diffraction angles ψ and ψ_0, especially near shadow boundaries. Small inaccuracies in these angles will lead to large errors in the total cross section pattern because of the sensitivity of the UTD coefficients near shadow boundaries at large distances.

VI. Acknowledgment

The authors would like to thank Melvin C. Gilreath and Thomas G. Campbell of NASA Langley Research Center for their interest and support of this project.

References

[1] J. B. Keller, "Geometrical theory of diffraction," *J. Opt. Soc. Am.*, vol. 52, pp. 116–130, Feb. 1962.

[2] R. G. Kouyoumjian, and P. H. Pathak, "A uniform geometrical theory of diffraction for an edge in a perfectly conducting surface," *Proc. IEEE*, vol. 62, no. 11, pp. 1448–1461, Nov. 1974.

[3] E. F. Knott, "A progression of high-frequency RCS prediction techniques," *Proc. IEEE*, vol. 73, no. 2, pp. 252–264, Feb. 1985.

[4] T. B. A. Senior and P. L. E. Uslenghi, "Comparison between Keller's and Ufimtsev's theories for the strip," *IEEE Trans. Antennas Propagat.*, vol. AP-19, no. 4, pp. 557–558, July 1971.

[5] E. F. Knott and T. B. A. Senior, "Comparison of three high-frequency diffraction techniques," *Proc. IEEE*, vol. 62, no. 11, pp. 1468–1474, Nov. 1974.

[6] P. Y. Ufimtsev, "Comments on 'Comparison of three high-frequency diffraction techniques'," *Proc. IEEE*, vol. 63, no. 12, pp. 1734–1737, Dec. 1975.

[7] R. A. Ross, "Radar cross section of rectangular flat plates as a function of aspect angle," *IEEE Trans. Antennas Propagat.*, vol. AP-14, no. 3, pp. 329–335, May 1966.

[8] C. E. Ryan and L. Peters, "Evaluation of edge-diffracted fields including equivalent currents for the caustic regions," *IEEE Trans. Antennas Propagat.*, vol. AP-17, pp. 292–299, May 1969.

[9] M. A. Plonus, "Radar cross section of curved plates using geometrical and physical diffraction techniques," *IEEE Trans. Antennas Propagat.*, vol. AP-26, no. 3, pp. 488–493, May 1978.

[10] C. L. Yu and J. Huang, "Air target analytical model," Naval Weapons Center, China Lake, CA, Int. Rep.

[11] F. A. Sikta, W. D. Burnside, T. Chu, L. Peters, "First-order equivalent current and corner diffraction scattering from flat plate structures," *IEEE Trans. Antennas Propagat.*, vol. AP-31, no. 4, pp. 584–589, July 1983.

[12] A. Michaeli, "Comments on 'First-order equivalent current and corner diffraction scattering from flat plate structures'," *IEEE Trans. Antennas Propagat.*, vol. AP-32, no. 9, pp. 1011–1012, Sept. 1984.

[13] F. A. Sikta, "UTD analysis of electromagnetic scattering by flat plate structures," Ph.D. dissertation, Ohio State Univ., 1981.

[14] T. Griesser, "Backscatter cross section of a dihedral corner reflector using GTD and PTD," M.S. thesis, Arizona State Univ., Dec. 1985.

[15] E. F. Knott, "RCS reduction of dihedral corners," *IEEE Trans. Antennas Propagat.*, vol. AP-25, no. 3, pp. 406–409, May 1977.

[16] A. Michaeli, "A closed form physical theory of diffraction solution for electromagnetic scattering by strips and 90° dihedrals," *Radio Sci.*, vol. 19, no. 2, pp. 609–616, Mar.-Apr. 1984.

[17] T. Griesser and C. A. Balanis, "Backscatter analysis of dihedral corner reflectors using the physical theory of diffraction," *IEEE Trans. Antennas Propagat.*, vol. AP-35, no. 10, pp. 1137–1147, Oct. 1987.

[18] C. A. Balanis, *Antenna Theory: Analysis and Design*. New York: Harper and Row, 1982, pp. 65–67, 118, 307–316, 502–522.

[19] K. M. Siegel, "Far field scattering from bodies of revolution," *Appl. Sci. Res.*, sec. B, vol. 7, p. 315, 1958.
[20] R. G. Kouyoumjian, "The geometrical theory of diffraction and its application," in *Numerical and Asymptotic Techniques in Electromagnetics*, R. Mittra, Ed., New York: Springer-Verlag, 1975.
[21] R. Tiberio and R. G. Kouyoumjian, "A uniform GTD solution for the diffraction by strips illuminated at grazing incidence," *Radio Sci.*, vol. 14, no. 6, pp. 933–941, Nov.-Dec. 1979.
[22] ——, "Calculation of the high-frequency diffraction by two nearby edges illuminated at grazing incidence," *IEEE Trans. Antennas Propagat.*, vol. AP-32, no. 11, pp. 1186–1196, Nov. 1984.
[23] R. Tiberio, G. Manara, G. Pelosi, and R. G. Kouyoumjian, "High-frequency diffraction by a double wedge," in *IEEE Antennas Propagat. Soc. Int. Symp.*, Vancouver, Canada, June 17–21, 1985, pp. 443–446.
[24] H. Shirai and L. B. Felsen, "High frequency multiple diffraction by a flat strip: Higher order asymptotics," *IEEE Trans. Antennas Propagat.*, vol. AP-34, no. 9, pp. 1106–1112, Sept. 1986.
[25] E. F. Knott, "RCSR guidelines handbook," EES/GIT Project A-1560-001, Eng. Experiment Station, Georgia Inst. Technol., Apr. 1976.

Timothy Griesser (S'85), for a photograph and biography please see page 1147 of the October 1987 issue of this TRANSACTIONS.

Constantine A. Balanis (S'62–M'68–SM'74–F'86), for a photograph and biography please see page 1147 of the October 1987 issue of this TRANSACTIONS.